Effect of mesoscopic out-of-plane defect on the fatigue behavior of a GFRP

Christophe Cruanes, Anwar Shanwan, Stéphane Méo, Samir Allaoui, Marie-Pierre Deffarges, Florian Lacroix, Gilles Hivet

Effect of mesoscopic out-of-plane defect on the fatigue behavior of a GFRP

C. Cruanes[a], A. Shanwan[b], S. Méo[a], S. Allaoui[b], M.-P. Deffarges[a], F. Lacroix[a], G. Hivet[b],

[a] Université de Tours, LMR, Tours, F-37200, France

[b] Université d'Orléans, PRISME, Orléans, F-45072, France

Abstract

This paper deals with the influence of buckles that are a mesoscopic out of plane defects on the fatigue behavior of a GFRP. Three cases were investigated: Healthy samples with no defect and specimens with buckles defects that are first generated in the longitudinal direction and then on the transverse direction.. First, static tests were used to measure the differences of the mechanical properties of both defect orientations and, thanks to digital image correlation, to see where were localized the areas of maximal local strain on the samples. Secondly, fatigue tests were performed in the three configurations. The results revealed that both defect orientations have a significant effect on the fatigue life and on the strain field. The configuration with defects in the transverse direction is the most crippling condition as expected from the static tests but the longitudinal direction configuration was also very affected by the presence of the mesoscopic defects. Those observations lead to conclude that this mesoscopic out of plane defect has a major negative influence on the fatigue life of such a composite.

Keywords

Defect, Process, Fatigue, Forming, Glass fibers

Introduction

The composites materials are widely used in the industry thanks to their very good mechanical characteristics for a lower mass than metal alloys. However, the processes developed in order to create the parts are complex and might induce defects, especially during textiles forming.

Those defects can be divided in two groups: macroscopic and mesoscopic (Figure 1). The macroscopic defects appear at the fabric scale. Among them, the most common and studied in the literature are the wrinkles. They highly depend on the fabric behavior and the boundary conditions. The first studies have limited the relationship between the limits of the mechanical behavior reached during the process and the wrinkles to the link between the in-plane shear behavior and the defect. Studies focused on the shear angle reached during the process compared to the locking angle described this relationship [1-4]. Recent numerical studies [5-7] shown that, because of being an out-of-plane phenomenon, the bending behavior of the membrane should be taken into account in order to correctly describe the shape and size of the wrinkles. A coupling between shear and tension has been highlighted in different papers [8-10] and wrinkles can therefore be avoided or delayed by applying tension along the yarn's network. Besides, wrinkles are the consequence of all strains and rigidities of the fabric and of the boundary conditions [10]. Wrinkles defects generate an over thickness that impact the geometrical tolerance and the aesthetics of the final part. Furthermore, studies have shown that this defect lead to a significant decrease of the composite performance, up to 40% loss of failure strength [11-13].

The second kind of defects, the mesoscopic defects, appears at the yarn level. Among those, there may be mentioned fibers and/or yarn breakage, "buckles", "weave pattern heterogeneity", "yarn waviness", etc… Some of these defects were only recently identified. Indeed, except for some work

on the phenomena involved during the appearance of defects like “yarn waviness”, “buckles” and “weave pattern heterogeneity”, there are few studies treating of the mesoscopic defects [10, 14-16]. Concerning the effect of the mesoscopic defects, except some studies on the effect of the fibre waviness on the UD composite [17-19], there are few studies to our knowledge on this aspect [21]. However, it has been shown that they are more recurring during complex preforms shaping [6, 10]. In addition, the inter-ply sliding increases significantly the amount and extent of these defects when multi-layered composite shaping is concerned [21], hence the need of understanding the phenomena involving and their criticality on the obtained composite.

This study is therefore in this framework and aims to evaluate the effect of the “buckles” defect on the composite mechanical properties and more precisely its fatigue behavior. For this, “buckles” have been generated on dry fabric layer taking care to reproduce the amplitudes observed on a complex composite part (Figure 1). Composite plates, of stacked layers at the same orientation, were then performed by injecting epoxy resin using resin transfer molding device. Plates without defects were also fabricated to be used as reference. Thereafter, uniaxial tensile tests and fatigue tests instrumented with digital image correlation devices were performed. Results of these different configurations were compared in order to evaluate the effect of “buckles” on the fatigue behavior of the composite.

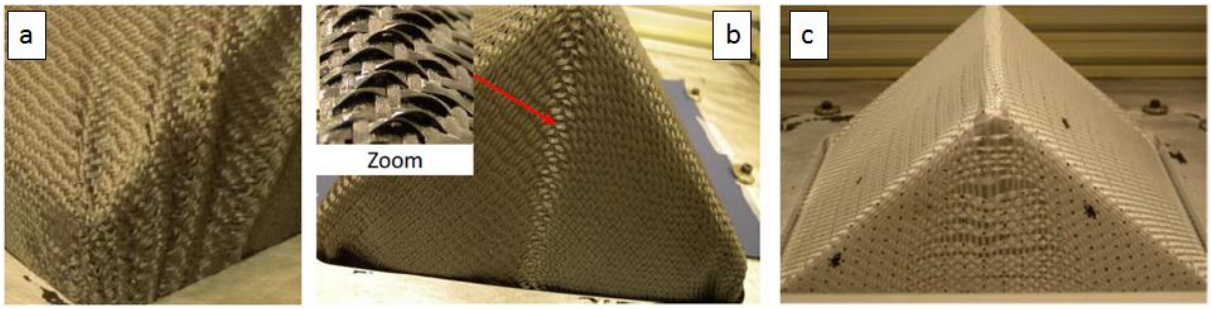

Figure 1 – Defects observed on double curved shape: (a) macroscopic (wrinkles), (b) mesoscopic (“buckles”) and (c) mesoscopic (“weave pattern heterogeneity”) – from [21]

1 Material and specimen preparation

.

1.1 Material

The material used in this study is a glass fiber reinforced polymer. Resin Transfer Molding process was used to produce composite plates, with and without defects, which were used to cut specimens. The fabric used is a glass plain weave produced by Chomarat Company. It is denoted G-WEAVE 600P and has the following properties: a real weight of 600 g / m2 ± 5%, thickness of 0.55 mm, warp and weft yarns count of 600 Tex. Thermosets epoxy resin LY564 ARALDITE with a suitable hardener 3487 ARADUR was used to inject staking performed according to the protocol described below. The fabric is balanced which was confirmed following DMA measurements performed on the GFRP which showed that the mechanical characteristics were similar along the warp and weft orientations.

1.2 Samples preparation

In order to produce plates without defects, the reinforcement was cut into square samples of 250×250 mm². The dimensions were selected to fit with the mold size. For plates with buckles defect, the reinforcement was cut into square samples of 500×500 mm². Then, the sample was placed on a machine equipped by four automated portal axes which can be commanded separately or simultaneously. The generation of the Buckle defects was obtained by applying a defined driving mode in the machine program. . The sample was held and fixed on the machine upon its three sides

(X, X’ and Y, Figure 2), then, a displacement at a constant velocity must be applied in the Y side (*y* axis) while the opposite side (Y’) must be free. Simultaneously, the two other sides, X and X’, must be piloted according to a force control order as a consequence, the two sides move towards the center of the sample.. Thanks to this type of control order, the reinforcement sample stretches in the Y direction and shrinks in the X and X' directions. After reaching the needed amplitude of defects, the sample is kept fixed and a fixing agent is sprayed on the surface of the sample. When the sprayed layer becomes dry, the calibrated sample can be removed and then cut into a square shape of 250×250 mm², as it is shown in Figure 2.

Several plies with calibrated defects have been produced according to this protocol. After that, staking of 7 plies oriented in the same direction was performed and placed in the RTM mold. Then, the epoxy matrix is injected and the mold transferred into a preheated oven at 100°C. After 3 hours, the mold was removed and kept cooling down at ambient temperature for 6 hours. The final thickness of the obtained composite plates is about 2.5 mm. Eventually, these plates were cut into several samples for the mechanical tests.

Those samples were all designed following the ISO 527-4 1B (Figure 3) allowing the use of lower capacity load cells and the localization of the damage in a central area of the sample, away from the clamps. They were cut out by waterjet cutting.

In the rest of the paper, the three configurations of sample for the mechanical tests will be named as follow (Figure 4):

Samples with No defect samples, or «ND» cut from the reference plates without defects and which will be taken as the reference (Figure 5-a).

Longitudinal defect samples, or « LD », cut along the area of the plates containing the calibrated buckle defects. The defect is placed on the central axis along the sample (Figure 5-b).

Transverse defect samples, or « TD », cut in the transverse direction of the plates with calibrated defects. The buckles are oriented at 90° with respect to the central axis of the sample (Figure 5-c) and are present only locally in an area on the center of the sample.

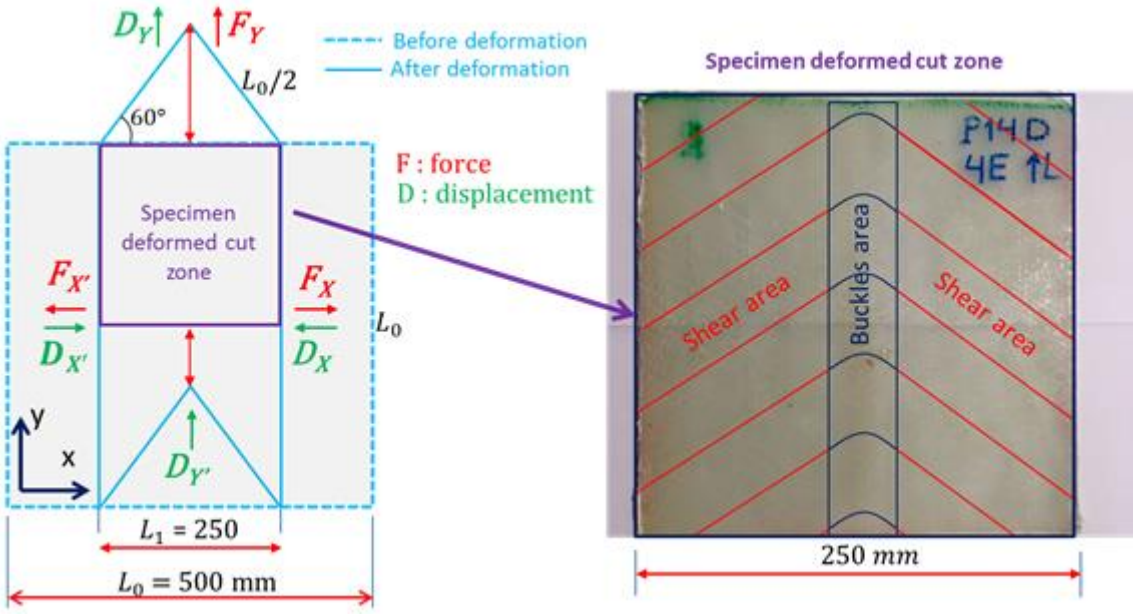

Figure 2 : Example for buckle defects generation

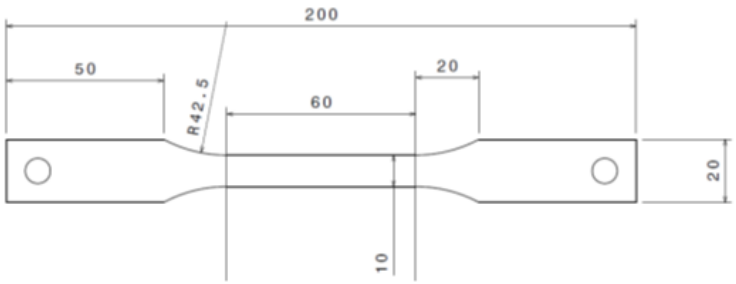

Figure 3 – Shape of the sample according to the ISO 527-4 1B (the dimensions are in mm). Thickness: 2,5mm

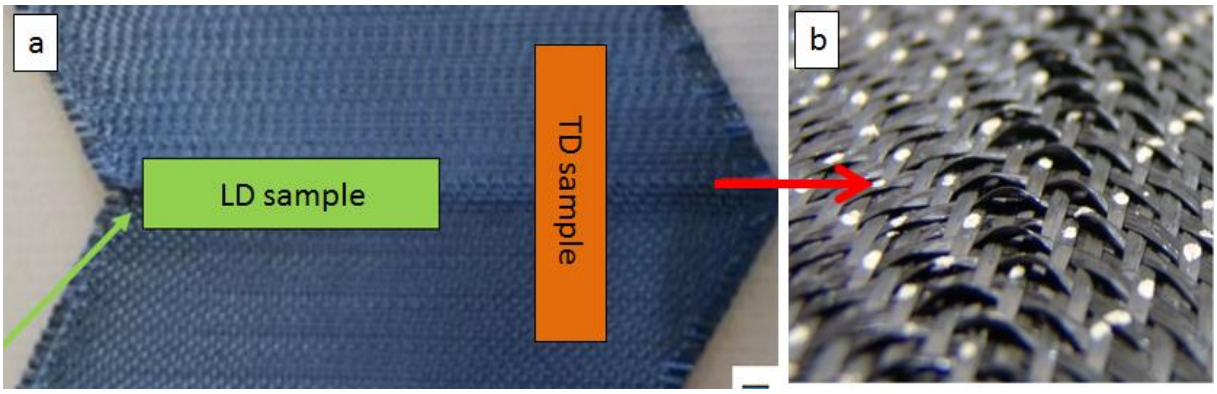

Figure 4 – (a) orientation of the cut of the LD and TD samples on the plate presenting a buckle defect. (b) zoom on the buckle defectFrom [21].

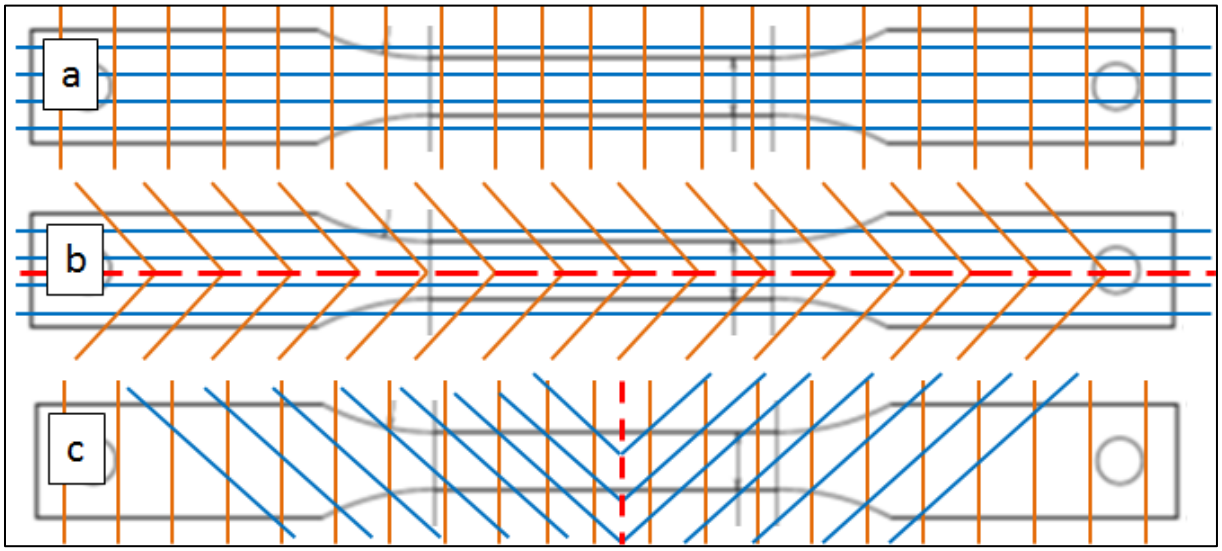

Figure 5 – Superposition of the grid of yarn on the sample in the three configurations: (a) ND, (b) LD and (c) TD. The red dotted line stands for the localization of the buckle defect.

2 Experimental protocol

In order to investigate the effect of the buckles mesoscopic defects and its orientation on the mechanical behavior of the GFRP, static and fatigue tests were performed. They were both conducted on an Instron 8872 servo-hydraulic fatigue testing machine at room temperature.

2.1 Digital Image Correlation

[11] showed that the impact of a ply defect could be monitored with a Digital Image Correlation (DIC) device. Therefore, in order to get the strain field and its evolution during the tests

investigated in this paper, a DIC system composed of two 5 million pixels CCD cameras (2448x2048 pixels) and the ARAMIS acquisition software have been used. The samples were prepared by firstly a layer of white paint and secondly a random pattern of dots with black paint in order to get a contrasted surface in front of the cameras.

2.2 Static tests

The static tests were displacement controlled at 2mm/min. The loading cells used were with a capacity of 25kN for the ND and LD samples and 5kN for the TD. The sampling used was 100Hz.

The frequency of the acquisition of the DIC for the static tests was 1Hz.

2.3 Fatigue tests

The fatigue tests carried out on the same machine as for the static tests, with the same loading cells. The tests were stress controlled, uniaxial, at 5Hz and with a 0.1 load ratio (defined as the ratio between the lowest and highest stress undergone by the sample during a cycle $\sigma_{min}/\sigma_{max}$) to ensure that the samples would not undergo buckling.

Table 1 shows the solicitations investigated for the three types of samples. The tests were carried out until failure of the sample and were chosen to cover from 50% of the ultimate stress σ_u, measured during the static test, to 25% of σ_u for the ND samples. For the two other types of samples, the tests started also at 50% of σ_u and then the maximum strain has been steadily decreased based on the fatigue life of previous solicitations. The lower solicitation for which a failure of the sample occurred was at 40% of σ_u for the TD and 25% of σ_u for the LD. A test was carried out at 25% of σ_u for the TD but was stopped after almost 12 million cycles without showing any sign of change in its fatigue behavior.

The strain was firstly directly measured by the fatigue machine and then corrected with DIC measurements every 20 minutes (or 10 minutes for the shorter tests) to take into account the compliance of the machine. Each DIC measurement lasted 30 seconds, or 150 cycles, over which the software recorded one image every 0.39s, or every 1.95 cycles, resulting in the recording of 75 images. This allowed the smoothing of the evolution of the results should there be a cycle where a punctual perturbation would occur. The values of strain then measured would be at a number of cycles taken as the mid value in the interval of cycles during which the measurement is conducted. The measurement couldn't be continuous, as the size of the files would be unmanageable.

	Maximum effort F_{max} (kN)	Maximum global stress σ_{max} (MPa)	Maximum global normalized stress $\frac{\sigma_{max}}{\sigma_{ult}}$	Fatigue life N_r (cycles)
LD samples	5	193,80	0,50	1250
	3	111,11	0,30	9763
	2,75	104,56	0,28	15734
	2,5	88,34	0,25	30713
	2,25	82,42	0,23	55402
	2	73,53	0,20	302000
	1,8	70,87	0,18	1035560
	1,6	62,99	0,16	20000
	1,25	46,30	0,13	4700000
TD samples	0,25	9,96	0,31	>11680000
	0,375	14,82	0,46	77400
	0,375	14,94	0,47	>2900000
	0,375	14,76	0,46	103539
	0,375	14,76	0,46	1029370
	0,375	15,12	0,47	954000
	0,4	16,13	0,51	222000
	0,4	15,59	0,49	43200
	0,4	15,94	0,50	52300
	0,4	16,13	0,51	895000
	0,4	15,33	0,48	13375
	0,45	18,07	0,57	95221
	0,45	17,51	0,55	12000
	0,45	18,99	0,60	25000
	0,45	18,07	0,57	546000
	0,5	20,41	0,64	139200
	0,5	20,33	0,64	18038
	0,5	19,46	0,61	12000
	0,5	20,62	0,65	13700
	0,5	20,16	0,63	17800
ND samples	6	220,59	0,49	8000
	5	190,84	0,42	14000
	4	151,52	0,34	86000
	4,5	163,64	0,36	41027
	4,5	163,64	0,36	48000
	3,5	132,08	0,29	277168
	3,35	127,38	0,28	1693820
	3,25	116,91	0,26	2077000
	3	112,78	0,25	3279000

Table 1 – List of the solicitations investigated in fatigue depending of the type of defect and the fatigue life associated. If the latter is in red, it means that the test was stopped before the failure.

3 Results

3.1 Static tests

The first step was to carry out static tests in order to estimate the ultimate stress on one sample for each considered configuration and also to see with digital image correlation (DIC) measurements where the areas of maximal localized strain are. Both information would then be useful for the fatigue part.

3.1.1 Mechanical response

The evolutions of the stress versus the strain during the static test for the three conditions are given on the Figure 6.

It can be observed that the ND and LD samples have close evolutions, moduli and ultimate stresses. [21] found out that the LD samples had even better mechanical characteristics than ND samples and explained this result as the consequence of the stiffness contribution of the transverse yarns, that undergoing the out of plane defect and consequently become not perpendicular with respect to the loading axis as shown on the Figure 5. This may be due the rotation angle of the transverse yarns over the specimen width may be very small in our case, which induces a zero contribution of rigidity. This variation is caused by the difference of the meso-architecture of the materials used in the two studies ad their mechanical behavior. In addition, the difference here is that only one static test was performed for each configuration. There is no way with those considerations to tell whether there is an increase or decrease of the mechanical characteristics. Therefore, and as the study focuses more on the fatigue aspects, it will be considered in the rest of the paper that the longitudinal orientation of the defect does not clearly impact the static characteristics of this GFRP.

The ND and LD also showed some damage in the area at the limit of the operational area of the sample, where the width goes from 10 to 20mm. This is an issue already observed ([22-23] for example), but it would not be met during the fatigue tests.

However, the TD sample differs greatly with much lower mechanical characteristics. This is again the consequence of the presence defect and the fact that there are no more yarns oriented in the loading direction as these yarns are those who are submitted to out of plane buckling and as a consequence they rotate on the areas adjacent to the defects (see Figure 5). All of these phenomena seem to cause a global weakening of the sample.

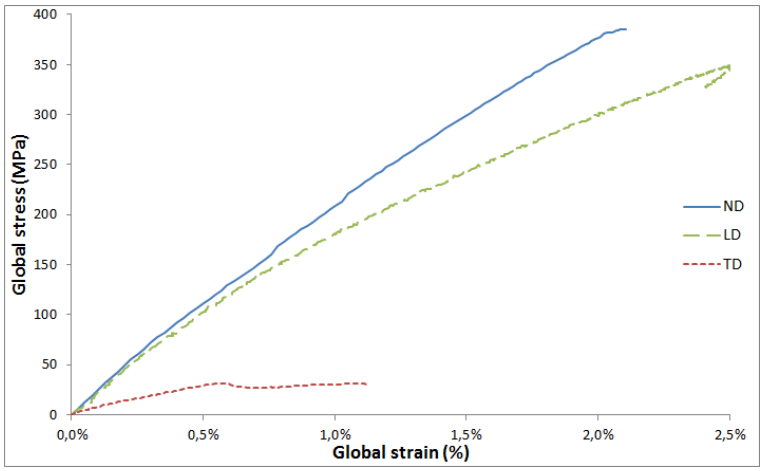

Figure 6 – Evolution of the stress versus the strain for the ND, LD and TD samples (1 test by curve)

3.1.2 DIC measurements

The Figure 7-8 show where are located the areas of maximal strain on each sample.

The ND sample showed that most of those areas are randomly dispatched in the central area of the sample. Many high local strain areas can be observed (Figure 7). The higher variations of strain (in yellow) are most probably caused by the plasticization of the matrix induced by the pattern of the yarns in the plies.

The LD sample showed many areas where the local strain is much higher than the global strain, with the most intense local strain on the sides of the sample (Figure 8). It seems that in those side areas (which are crossed by the paths 1 and 3) the local strain increased much faster than in the

central area (even if in the latter it can reach 3 times the global strain). Indeed, that is in those side areas that cracks can be seen while it is still the seemingly elastic phase of the test. With the LD configuration, the mechanical properties remain close to the ND configuration at the cost of the presence of many cracks in the sample in the sample at an early stage.

The TD sample showed two areas where the local strain is much higher than the global strain (Figure 9). Those areas are located in the surrounding of the defect, where the cracks are exclusively met. The lower mechanical properties are well explained as the local strain in the areas is almost 20 times higher than the global strain on the Figure 9-B.

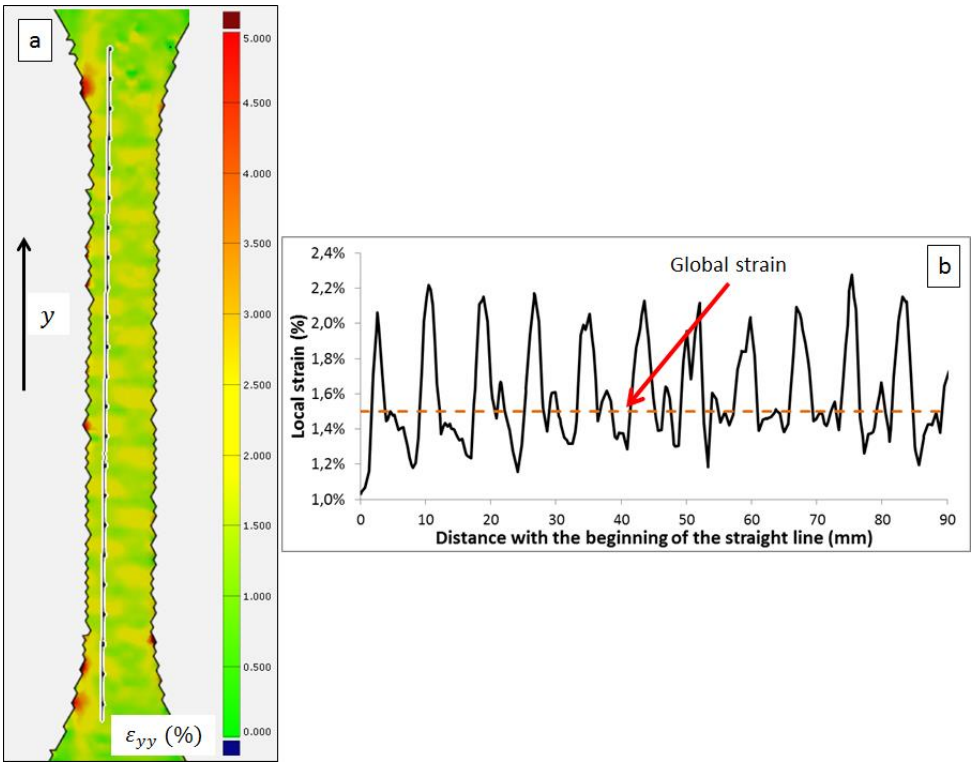

Figure 7 – ND sample: local strain field measured with DIC during the static test while the global strain is 1.5% (a). (b) shows the evolution of the local strain alongside the path depicted in the figure (a).

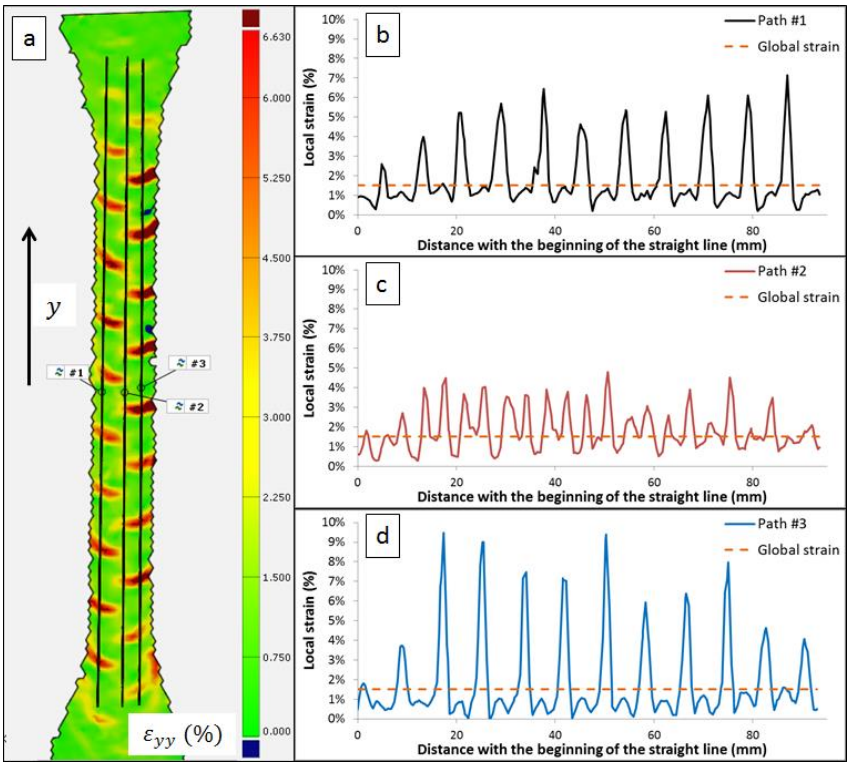

Figure 8 – LD sample. Local strain field measured with DIC during the static test while the global strain is 1.5% (a). (b) (respectively (c) and (d)) shows the evolutions of the local strain alongside the path #1 (resp. #2 and #3) in the figure (a).

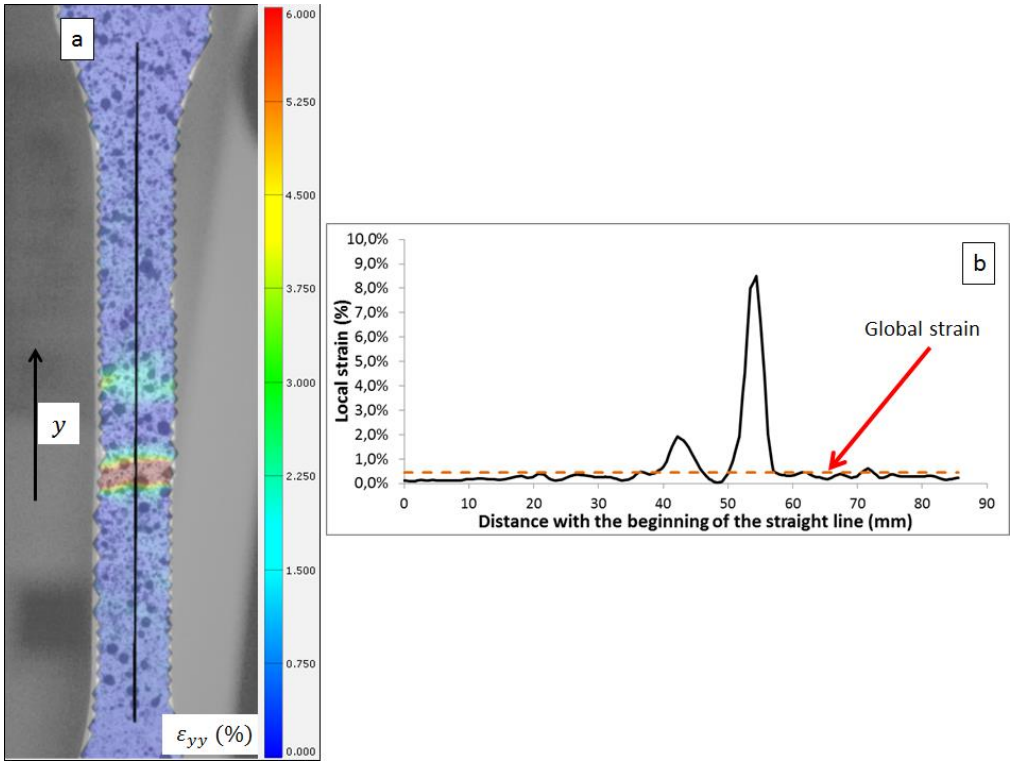

Figure 9 – TD sample: local strain field measured with DIC during the static test while the global strain is 0.46% (a). (b) shows the evolution of the local strain alongside the path depicted in the figure (a).

3.2 Fatigue tests

The static tests gave access for each type of sample to the ultimate stress and their capacity to produce an area of strain concentration which would be the most likely to see the occurrence of cracks.

3.2.1 Wöhler curves

The Wöhler curve for each sample is drawn on the Figure 10. All the samples show a classical evolution divided in two parts: low (LCF) and high cycle fatigue (HCF). The equation of the logarithmic evolution during the LCF phase is also plotted (dotted line). The two phases are differentiated by the type of damage the sample undergoes: the static-fatigue damage is predominant during the LCF phase, whereas the fatigue-fatigue damage is predominant during the HCF phase [24].

3.2.1.1 ND samples

The ND showed an evolution with a limit between LCF and HCF around 29% of the ultimate stress, at a stress of 132MPa.

It can be observed on the Figure 11 that the stiffness decreased during fatigue tests. Two phases can be identified: a slow decrease followed by a faster one until the failure of the sample. The intensity of the first phase depends on the solicitation: the stronger the maximum stress, the stiffer the slope. The reason for this first slow decrease is that the pattern followed by the yarns (taffeta) generates some local plasticization as seen on the Figure 7, implying that the matrix will creep. Then, at some point during the test, cracks appeared and propagated, accelerating the decrease of the stiffness [25-26].

The DIC observations showed that for the lower solicitations, lower than de LCF/HCF limit, there are many areas where the local strain is many times higher than the global strain (see 3.1.2) as can be seen on the Figure 12. Those areas are most likely plasticized and will eventually lead to the appearance of surface cracks. For the higher solicitations, there are fewer cracks (2 or 3 at top) which initiated from one of the plasticized areas.

3.2.1.2 TD samples

The TD samples were expected to have the lowest fatigue characteristics among the three types of sample given the static tests. The limit between low and high cycle fatigue is close to 45% of the ultimate stress, at a stress of 14MPa.

It can be seen that the areas of maximum strain are in the neighborhood of the defect, which is the same as in static. The DIC observations showed that the cracks initiated for all the samples in one of the two areas, which is logical as the maximum local strain measured is much higher than the global maximum strain recorded on a cycle. Indeed, the Figure 13 shows that for a test at 15MPa with a fatigue life of 10^6 cycles, the ratio of the maximum local and global strain at the 510000^{th} cycle is around 16. It appears that for the TD samples, the average ratio is around 22.15.

The rest of the sample showed very little variation in the field of strain, which is expected as the solicitation undergone by the TD samples are very low compared to those of the ND campaign (20MPa maximum versus 220MPa maximum).

3.2.1.3 LD samples

The fatigue characteristics of the LD samples are lower than ND with a LCF/HCF limit between 20% and 22% of the ultimate stress, at a stress around 78MPa.

The areas of maximum strain, shown on the Figure 14, can be divided in two groups. The first one is composed of areas located on both edges of the sample, at the same spot as the areas of maximum

strain observed in static (Figure 8). However, the sample fails before they reach a comparable size with the static ones. It is caused by the appearance of a second group of areas of maximum deformation positioned on the center of the surface of the sample. The areas of this second group are regularly distributed along the center axis of the sample, where the warp yarns make an angle (Figure 2). Those observations relate very well with the distinction between static-fatigue and fatigue-fatigue damage as already discussed in the literature [22, 27-29].

3.2.1.4 Comparisons between the ND samples and the defected samples

Beforehand, let's introduce the LMS/GMS ratio. At the number of cycles where the stiffness starts to plummet, the Local and Global Maximum Strain (LMS and GMS) were measured, using the DIC, over this cycle and a ratio LMS/GMS has been calculated (Table 2).

Comparison between ND and TD:

The fatigue behavior of the ND and TD samples is qualitatively different: the LCF/HCF limit of the TD samples was for a maximum stress leading to 1'000'000 cycles, whereas for the ND samples it was around 200'000 cycles. The slope of the LCF line is lower for the TD than the ND (Figure 10).

The TD samples see a more localized damage than the ND samples. While the maximum stress and the maximum global strain were much lower for the TD, the local maximum strain is much higher. Indeed LMS/GMS ratio was measured between 11.53 and 32.94 for the TD (average value of 22.15) whereas it was between 3.79 and 17.33 for the ND (average value of 8.06) (Table 2). It is also interesting to note that the LCF/HCF limit increased from $0.29.\sigma_u$ (ND) to $0.45.\sigma_u$ (TD).

The presence and the orientation of the defect have a substantial influence on the mechanical characteristic, being static or fatigue, causing the yarns to be less efficient and the matrix to work more than in the normal configuration.

Comparison between ND and LD:

They both have the same fatigue behavior, with a LCF/HCF limit for a maximum stress leading to fatigue life around 200'000 cycles. Moreover, the slope of the LCF line is roughly the same (Figure 10).

However, the LD samples see more damage than the NDs. Indeed, for a test at 111.1MPa, the fatigue life is $3.1.10^6$ cycles for the ND whereas it is 10^4 cycles for the LD. It also appeared from the DIC observations that the yarn network in the LD induced plasticization and eventually damage in the sample as the LMS/GMS ratio was much more important: from 5.54 to 16.75 for the LD (average value of 11.54) compared to the range from 3 to 17 for the ND (average value of 8.06) (Table 2).

The consequence of the presence of the buckle mesoscopic defects in the LD configuration is that it creates around the central axis of the sample a source of delamination which was more outlined than on the ND samples (Figure 15).

It is worth noting that if the presence of the defect with this orientation has very much impact on the static behavior [21], it has a major effect on the fatigue behavior [30-31] by enabling the delamination in the sample. Thus, it explains the differences between the behaviors of both types of samples [32].

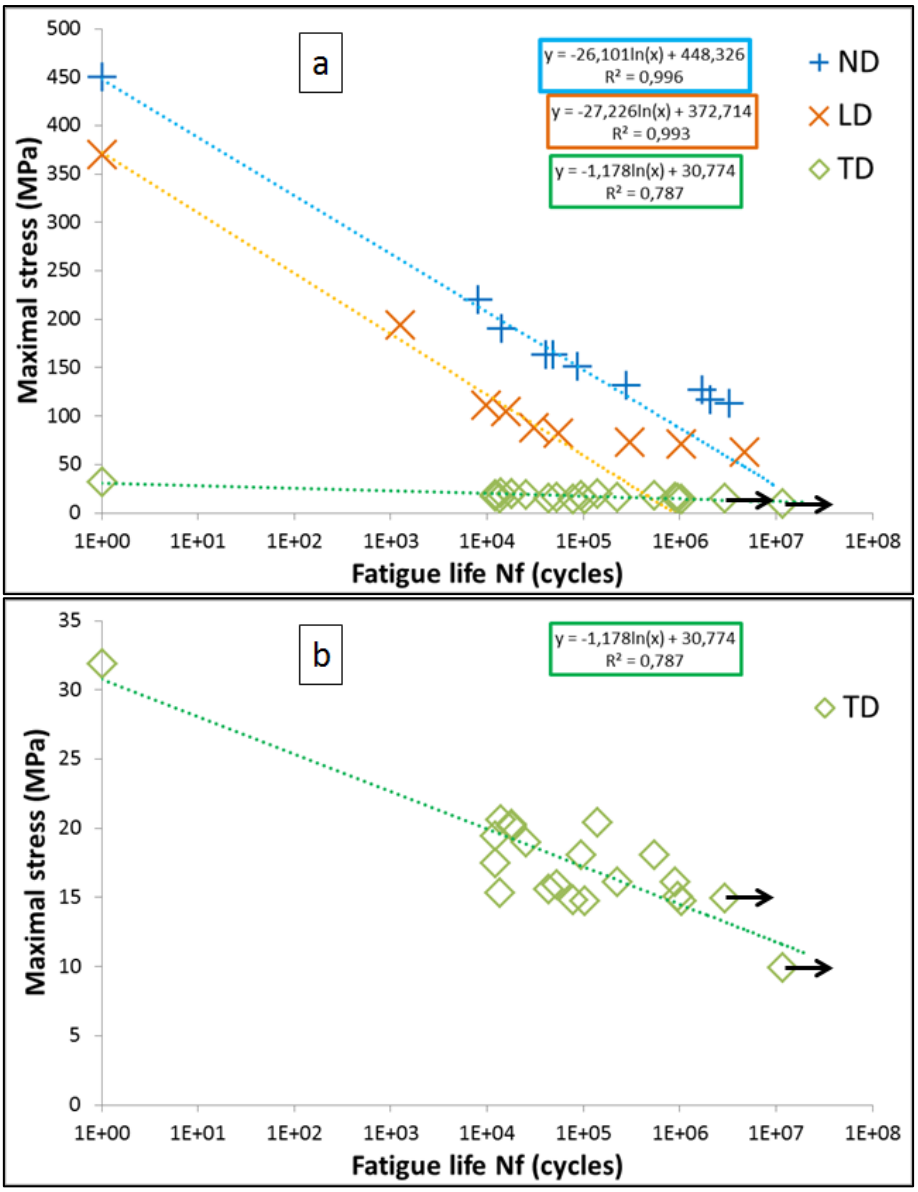

Figure 10 – Wöhler curve for each sample in a maximum stress/fatigue life chart (a). The chart (b) shows a zoom on the TD Wöhler curve. The dotted lines represent the fatigue behavior during the LCF phase.

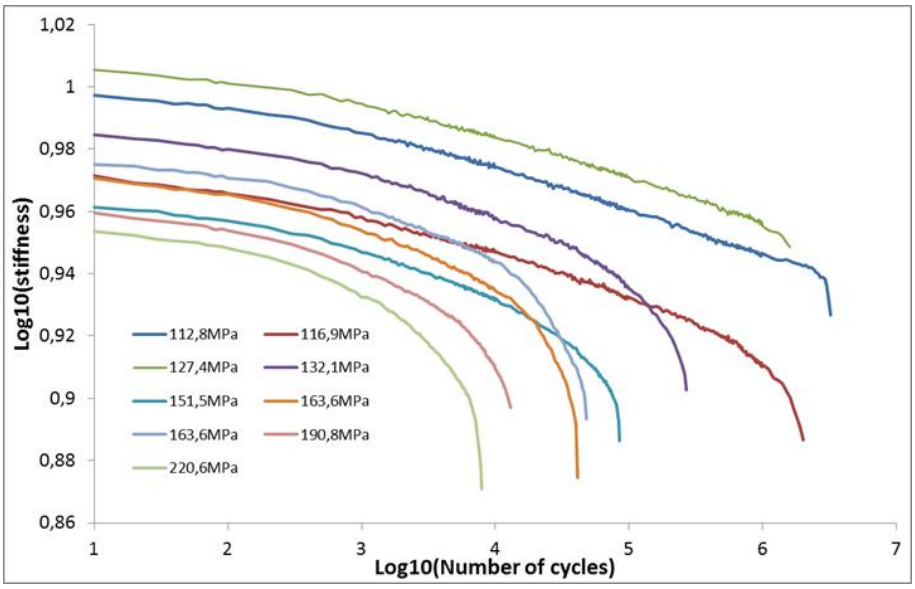

Figure 11 – Evolution of stiffness during the fatigue tests on the ND samples in a log/log chart.

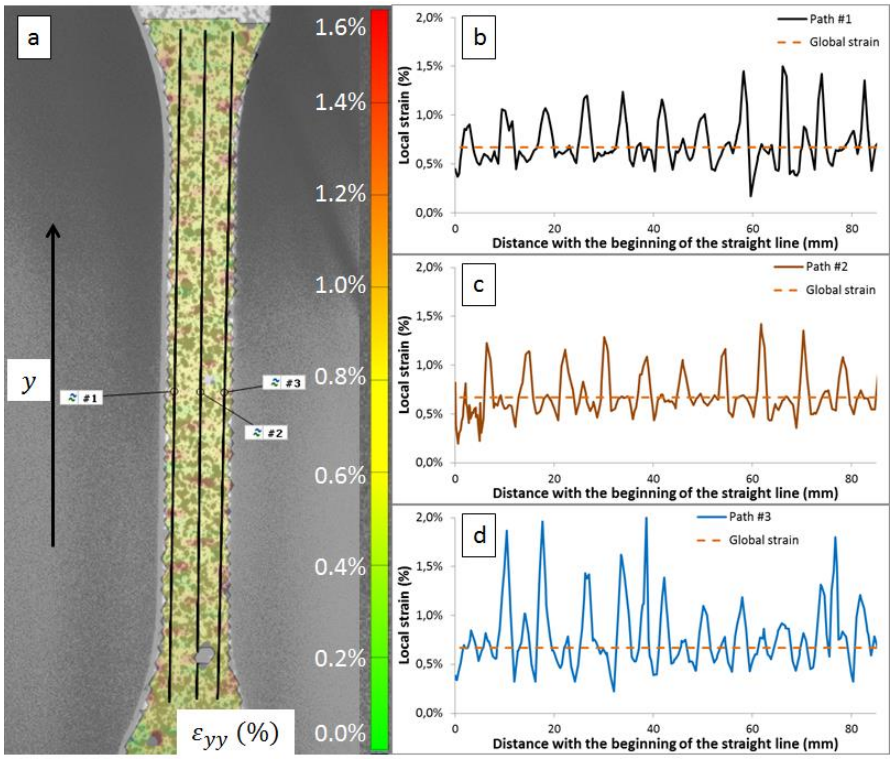

Figure 12 – (a) Example of strains distribution on a ND sample during a fatigue test ($\sigma_{max} = 127,4\ MPa, N = 510000\ cycles, \varepsilon_{glob} = 0,67\%$). (b), (c) and (d) show the evolution of the local strain alongside the path #1, #2 and #3.

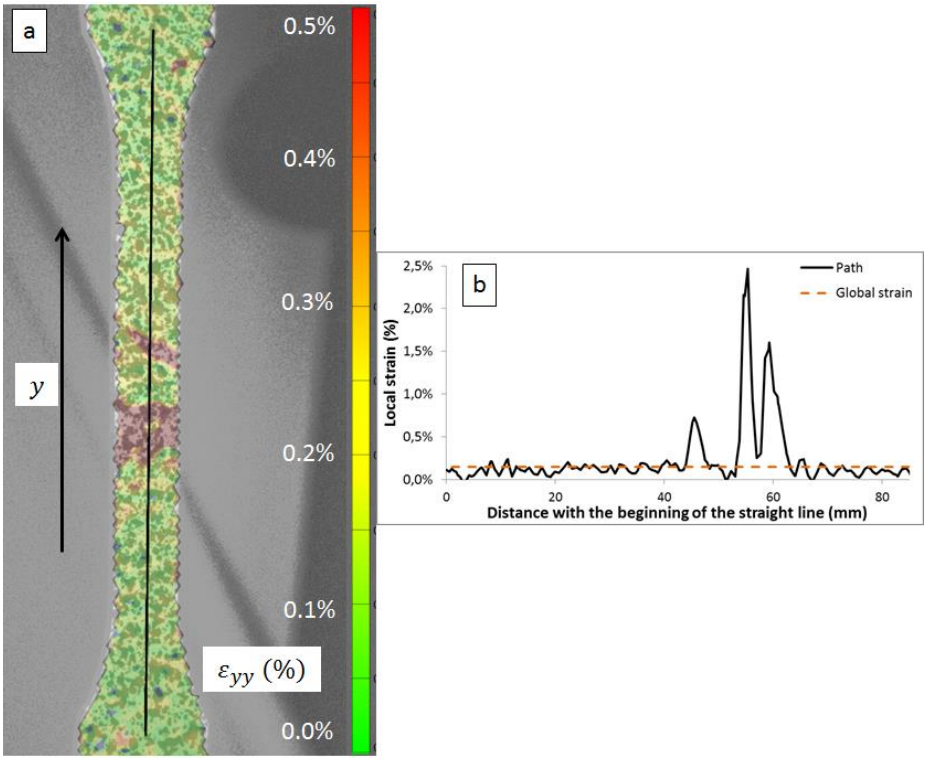

Figure 13 – (a) Measurements of the local and global maximal strain on a TD sample ($\sigma_{max} = 15\ MPa, N = 510000\ cycles, \varepsilon_{glob} = 0,15\%$). (b) shows the evolution of the local strain alongside the path depicted on the figure (a).

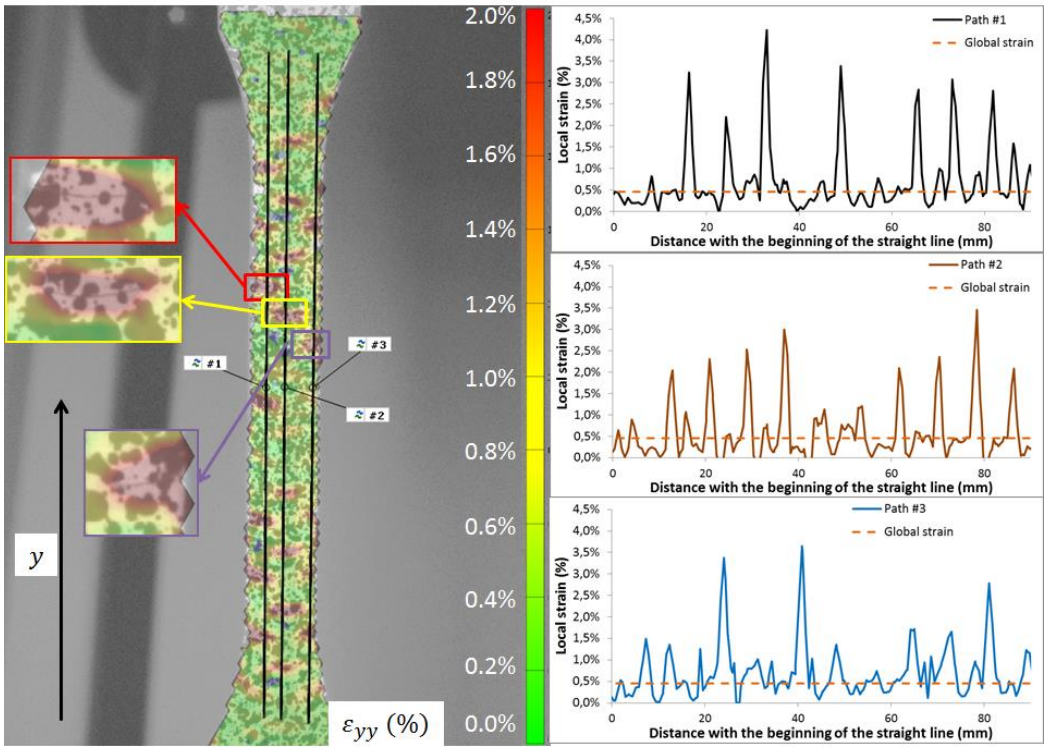

Figure 14 – (a) DIC measurements of the local strain on a LD sample ($\sigma_{max} = 70,9\ MPa, N = 620000\ cycles, \varepsilon_{glob} = 0,45\%$). (b), (c) and (d) show the evolution of the local strain alongside the path #1, #2 and #3.

Figure 15 – View of the side of LD samples with short fatigue life: $\sigma_{max} = 194\ MPa$ (a) and $\sigma_{max} = 111\ MPa$ (b)

	Global stress (MPa)	Local maximum strain LMS (%)	Global maximum strain GMS (%)	$\frac{LMS}{GMS}$
LD Samples	193,80	--	--	--
	111,11	19,37%	1,16%	16,75
	104,56	4,05%	0,58%	7,03
	88,34	5,21%	0,76%	6,82
	82,42	8,82%	0,53%	16,51
	73,53	2,83%	0,22%	12,96
	70,87	6,81%	0,45%	15,13
	62,99	--	--	--
	46,30	1,19%	0,22%	5,54
TD Samples	20,41	--	--	--
	20,33	3,35%	0,17%	20,19
	19,46	4,10%	0,19%	22,16
	20,62	4,00%	0,20%	20,41
	20,16	--	--	--
	16,13	--	--	--
	15,59	4,38%	0,13%	32,94
	15,94	3,06%	0,15%	19,84
	16,13	3,75%	0,15%	24,64
	15,33	6,83%	0,23%	29,18
	14,82	4,50%	0,16%	28,13
	14,94	--	--	--
	14,76	1,74%	0,15%	11,53
	14,76	3,57%	0,15%	24,29
	15,12	1,41%	0,14%	10,40
	9,96	--	--	--
ND Samples	220,59	15,91%	1,39%	11,45
	190,84	10,96%	1,20%	9,11
	163,64	5,39%	1,01%	5,34
	163,64	7,20%	1,02%	7,09
	151,52	16,14%	0,93%	17,33
	132,08	4,49%	0,79%	5,66
	127,38	2,54%	0,67%	3,79
	116,91	5,84%	0,73%	8,05
	112,78	2,90%	0,62%	4,70

Table 2 – Maximal local and global strain

4 Conclusion

Static and fatigue tests were carried out on a GFRP with and without an induced out of plane mesoscopic defects. The orientation of this defect has also been investigated.

The 0° orientation defect (LD) showed that, despite a close static behavior, the induced defects had a very important influence on the fatigue behavior, with lower stress investigated. The use of digital image correlation allowed observing that the number of cracks and the ratio of local strain over global strain was also much higher than on the healthy samples. It can be then concluded that the presence of the defect with this orientation would make the sample more likely to undergo delamination.

However, the 90° orientated defect (TD) showed the same influence of the presence of the defect on the behavior in static and in fatigue: it would catastrophically decrease the mechanical characteristics.

Only two orientations, at a given buckles amplitude, were tested in this study. As they are the two extremes cases, it is possible to say that the presence of this buckle mesoscopic defects in the

composite, whatever the orientation, would have a non-negligible influence on the fatigue behavior. It would not even need to be on an important area as it would be a site where the delamination would most likely initiated.

More information could be given on the damage seen by the samples, with scanning electron microscopy on the areas where the out of plane defects induce an important local strain for example.

Acknowledgment

The authors wish to thank Centre-Val-de-Loire Region for its financial support in the project IDDEFORM. They also would thank the team from the CERMEL and more particularly Mathieu Venin for his precious help.

References

1. Wang J., Paton R., Page J.R. The draping of woven fabric preforms and prepregs for production of polymer composite components. Composites: Part A, 1999; 30:757-765

2. Potluri P., Sharma S., Ramgulam R. Comprehensive drape modeling for molding 3D textile preforms. Composites: Part A, 2001; 32:1415-1424

3. Prodromou A.G.,Chen K. On the relationship between shear angle and wrinkling of textile composite preforms. Composites: Part A, 1997; 28:491-503

4. Sharma S.B., Sutcliffe M.P.F., Chang S.H. Characterization of material properties for draping of dry woven composite material. Composites: Part A, 2003; 34:1167-1175

5. Hamila N., Boisse P. Simulations of textile composite reinforcement draping using a new semi discrete three node finite element. Composites: Part A, 2008; 39:999-1010

6. Allaoui S., Boisse P., Chatel S., Hamila S., Hivet G., Soulat D., Vidal-Salle E. Experimental and numerical analyses of textile reinforcement forming of a tetrahedral shape. Composites: Part A, 2011; 42:612-622

7. Ten Thije R.H.W., Akkerman R., Huétink J. Large deformation simulation of anisotropic material using an updated lagrangian finite element method. Comp. Meth. In App. Mech. & Eng., 2007; 196:3141-3150

8. Boisse P., Hamila N., Vidal-Sallé E., Dumont F. Simulation of wrinkling during textile composite reinforcement forming. Influence of tensile, in-plane shear and bending stiffness. Compos. Sci. Tech., 2011; 71:683-692

9. Wilems A., Lomov S., Verpoest I., Vandepitte D., Harrison P., Yu W. Forming simulation of a thermoplastic commingled woven textile on a double dome. Int.Jour. of Mat. Form., 2008; 1:965-968

10. Allaoui S., Hivet G., Soulat D., Wendling A., Ouagne P., Chatel S. Experimental performing of highly double curved shapes with a case corner using an interlock reinforcement. Int. J. Mater. Form., 2014; 7:155-165

11. Bloom L.D., Wang J., Potter K.D. Damage progression and defect sensitivity: an experimental study of representative wrinkles in tension. Composites: Part B, 2013; 45:449-458

12. Hallander P., Akermo M., Mattei C., Petersson M., Nyman T. An experimental study of mechanisms behind wrinkle development during forming of composite laminates. Composites: Part A, 2013; 50:54-64

13. Potter K., Khan B., Wisnom M., Bell T., Stevens J. Variability, fibre waviness and misalignment in the determination of the properties of composite materials and structures. Composites: Part A, 2008; 39:1343-1354

14. Lightfoot J.S., Wisnom M., Potter K. Defects in woven preforms: formation mechanisms and the effects of laminate design and layup protocol. Composites: Part A, 2013; 51:99-107

15. Härtel F., Middendorf P. Process parameters studies and comparison of different preform processes with NCF material. In proceeding of ICCM-19. Montreal, July, 2013

16. Gatouillat S., Bareggi A., Vidal-Sallé E., Boisse P. Meso modelling for composite preform shaping – simulation of the loss of cohesion of the woven fibre network. Composites: Part A, 2013; 54:135-144

17. Hsiao H.M., Daniel I.M. Elastic properties of composites with fibre waviness. Composites: Part A, 1996; 27:931-941

18. Piggott M.R. The effect of fiber waviness on the mechanical properties of unidirectional fibre composite: a review. Comp. Sci. & Tech., 1995; 53:201-205

19. Wang J., Potter K., Hazra K., Wisnom W. Experimental fabrication and characterization of out-of-plane fiber waviness in continuous fiber-reinforced composites. Jour. of Comp. Mat., 2012; 46:2041:2053

20. Allaoui S., Cellard C., Hivet G. Effect of inter-ply sliding on the quality of multilayer interlock dry fabric. Composites: Part A, 2015; 68:336-345

21. Allaoui S., Hivet G., Haddad M., Agogué R., Khellil K., Beauchene P., Aburra Z., Effect of the buckles mesoscopic defects on the composite properties. In ICCM-20. Copenhagen, July, 2015.

22. Garcea S.C., Mavrogordato M.N., Scott A.E., Sinclair I., Spearing S.M. Fatigue micromechanism characterization in carbon fibre reinforced polymers using synchrotron radiation computed tomography. Comp. Sci. Tech., 2014; 99:23-30

23. Garcea S.C., Sinclair I., Spearing S.M. In situ synchrotron tomographic evaluation of the effect of toughening strategies on fatigue micromechanisms in carbon fibre reinforced polymers. Comp. Sci. Tech., 2015; 109:32-39

24. Epaarchchi J.A. Effects of static-fatigue (tension) on the tension-tension fatigue life of glass fibre reinforced plastic composites. Comp. Struct., 2006; 74:419-425

25. Demers C.E. Tension-tension axial fatigue of E-glass fiber-reinforced polymeric composites: tensile fatigue modulus. Constr. Build. Mat., 1998; 12(1):51-58

26. Montesano J., Fawaz Z., Bougherara H. Non –destructive assessment of the fatigue strength and damage progression of satin woven fiber reinforced polymer matrix composites. Composites: Part B, 2015; 71:122-130

27. Reifsnider K.L. Damage and damage mechanics In: Raifsnider KL, editor. Fatigue of composite materials. Amsterdam: Elsevier; 1990

28. Phoenix S.L. Modeling the statistical lifetime of glass fiber/polymer matrix composites in tension. Comp. Struct., 2000; 48:19-29

29. Beaumont P.W.R., Sekine H. Physical modeling of engineering problems of composites and structures. Appl. Comp. Mat., 2000; 7:13-37

30. Colombo C., Vergani L. Influence of the delamination on fatigue properties of a fiberglass composite. Comp. Struct., 2014; 107:325-333

31. Reis P.N.B., Ferreira J.A.M., Antunes F.V., Richardson M.O.W. Effect of interlayer delamination on mechanical behavior of carbon/epoxy laminates. J. of Comp. Mat., 2009; 43:2609-2621

32. Dyer K.P., Isaac D.H. Fatigue behavior of continuous glass fibre reinforced composites. Composites: Part B, 1998; 29:725-733